Available online at www.sciencedirect.com

ScienceDirect

ARTICLE

Analysis on Crack Driving Force at Stress Corrosion Cracking Tip Induced by Scratch in Nickel-based Alloy

Zhao Lingyan,   Cui Yinghao,   Yang Fuqiang,   Xue He

Xi'an University of Science and Technology, Xi'an 710054, China

Abstract: To understand the effects of the oxide morphology on the crack tip of scratched surface on stress corrosion cracking (SCC) behavior of nickel-based alloy, the local stress-strain field at scratched crack tip in the presence of film-induced stress was simulated. Results show that wedge force is the major crack driving force that causes the SCC growth. Greater oxide thickness of scratch crack will give rise to larger wedge force and lead to an increase in SCC crack growth rate (CGR). The formation of oxide at crack tip will induce compressive stress, compressive strain and negative strain gradient, and thus retard the SCC propagation in the upper and lower part of the semi-elliptical crack front.

Key words: nickel-based alloy; scratch; oxide morphology; wedge force; crack growth rate (CGR)

Due to their protective role of chromium oxide on the material surface, nickel-based alloys are commonly used to fabricate transfer tubes of pressurized water vapor generators. However, surface scratches, which are prone to appear during manufacture, transport and installation of steam generator[1,2], are one of the origins of stress corrosion cracking (SCC) in steam generators[3,4], and seriously threaten the safety and reliability of nuclear power plant. Generally, SCC is the degradation of materials under the combined actions of load, material and corrosive medium. The SCC propagation is very slow but the SCC that initiates and propagates at scratch banks and grooves always appears suddenly. During the SCC process, an additional tensile stress, which exists at the substrate side of substrate-oxide film interface, plays an important role in the formation of deep crack. The additive stress generated by the formation of oxides on the surface of base metal and the applied loads, will enhance the dislocation emission and motion. Microcracks induced by surface scratch will initiate when the corrosion-enhanced dislocation emission and motion reach a certain condition[5,6]. In the rupture and rebuilt process of oxide formed around surface scratches, microcracks will propagate together with the continuous transformation of oxide morphology.

Mechanical status at crack tip is one of the key factors in the analysis of SCC mechanism and quantitative prediction of crack growth rate (CGR) of nickel-based alloys SCC for nuclear pressure vessels and steam generators[7]. However, the effects of the oxide morphology at scratched surface on SCC behavior of nickel-based alloy have not been investigated and understood. Based on a finite element method (FEM) and sub-model technology, in the presence of film-induced stress, the crack tip mechanical field of scratched nickel-based alloy 600 has been analyzed. The influence of oxide morphology on the SCC initiating and propagating behaviors was also analyzed. Combined with the film slip/dissolution oxidation model, the CGR of scratched nickel-based alloy 600 with different oxide morphology was calculated. The primary object is to gain some understanding for the direct influence of oxide morphology on the mechanochemical effect in SCC process of scratched nickel-based alloy.

1   Theoretical Basis

The film slip/dissolution oxidation model is widely regarded as a reasonable description of SCC growth

estimation in the nickel-based alloys in high temperature oxygenated environment[8]. In this model, the SCC growth rate can be written as:

$$\frac{da}{dt} = \kappa_a \left(\dot{\varepsilon}_{ct} \right)^m \tag{1}$$

where, κ_a is the oxidation rate constant, which is determined by the electrochemical environment and material property in the vicinity of the crack tip; m is the exponent of current decay curve, whose value is related to the measurable parameters including corrosion potential, solution conductivity, and a degree of chromium depletion in the electrochemical environment; $\dot{\varepsilon}_{ct}$ is the strain rate at a fixed distance ahead of crack tip, which can be written as $d\varepsilon_{ct}/dt$.

And the oxidation rate constant κ_a is given by,

$$\kappa_a = \frac{M_{mol}}{\rho F z} \cdot \frac{i_0}{1-m} \cdot \left(\frac{t_0}{\varepsilon_f} \right)^m \tag{2}$$

where M_{mol} is the molecular weight of the metal; ρ is the density of the metal; F is Faraday's constant; z is the change in charge due to the oxidation process; i_0 is the oxidation current density of the bare surface; t_0 is the time before onset of the current decay and $\dot{\varepsilon}_f$ is the degradation strain of the oxide film.

It is very difficult to obtain the strain rate at the crack tip exactly in Eq.(1), so the tensile plastic strain $\dot{\varepsilon}_p$ is proposed to substitute the tensile plastic strain ε_{ct} at a characteristic distance r_0 in front of the crack tip, which can be written as

$$\varepsilon_{ct} = \varepsilon_p \Big|_{r=r_0} \tag{3}$$

where, r is the distance in front of the crack tip, whose variation will cause the increase of crack tip strain when the crack is growing.

$$\frac{d\varepsilon_{ct}}{dt} = \frac{d\varepsilon_p}{dt} = \frac{d\varepsilon_p}{da} \cdot \frac{da}{dt} \tag{4}$$

where, $d\varepsilon_p/da$ is the strain rate at a characteristic distance r_0 in front of the growing crack tip.

Substituting Eq.(4) into Eq.(1), the SCC growth rate at the crack tip in a high temperature oxygenated aqueous system can be expressed as

$$\frac{da}{dt} = \left(\kappa_a \right)^{\frac{1}{1-m}} \cdot \left(\frac{d\varepsilon_p}{da} \right)^{\frac{m}{1-m}} = \kappa_a' \cdot \left(\frac{d\varepsilon_p}{da} \right)^{\frac{m}{1-m}} \tag{5}$$

where $\kappa_a' = \left(\kappa_a \right)^{\frac{1}{1-m}} \tag{6}$

Considering the strain re-distribution at a growing crack tip, based on the strain gradient theory, Shoji[9] suggested the expression written as follows,

$$\frac{d\varepsilon_p}{da} = \frac{\partial \varepsilon_p}{\partial a} - \frac{\partial \varepsilon_p}{\partial r} \tag{7}$$

The stress intensity factor is invariant at a steadily growing crack tip, then the first term of Eq.(7) can be omitted, and finally Eq.(7) can be written as

$$\frac{d\varepsilon_p}{da} = -\frac{\partial \varepsilon_p}{\partial r} = -\frac{d\varepsilon_p}{dr} \tag{8}$$

Substituting Eq.(8) into Eq.(5), the SCC growth rate can be expressed as

$$\frac{da}{dt} = \kappa_a' \cdot \left(\frac{d\varepsilon_p}{dr} \right)^{\frac{m}{1-m}} \tag{9}$$

Eq.(9) can be used as the basic formula to quantitatively estimate SCC growth at flaws in actual LWR components[10], and the variation of tensile plastic strain with crack growth $d\varepsilon_p/dr$ at a characteristic distance r_0 can be considered as the unique mechanical factor affecting SCC crack behavior. Combined with the elastic-plastic FEM, a pre-analytical method is used to calculate the plastic strain gradient $d\varepsilon_p/dr$ at a characteristic distance r_0, then the SCC growth rate at a crack tip or along the crack front can be estimated. It must be mentioned that the characteristic distance r_0 is a very important parameter in this approach. However, it is still not very clear to how to determine the value of r_0, which has more to do with the SCC growth mechanism[11]. For a regular electrochemical environment where the crack tip is exposed, the plastic strain gradient at crack tip is essentially consistent with CGR.

2 Finite Element Model

2.1 Specimen and geometry model

Alloy 690TT is susceptible to SCC in high temperature oxygenated water. Therefore its cross-section morphology was formed by a scratch technique in high temperature oxygenated water at 325 ºC after a constant load experiment, which demonstrated the SCC crack initiation in Fig.1[2]. Mechanical cracks were produced at the bottom of scratch groove during slow strain rate tensile stage. The mechanical cracks, whose tips were highly approached to or along the grain boundaries, could be the precursor for SCC crack initiation and propagation. The oxides were also formed on scratch groove.

To study the micro-mechanical state at SCC crack tip induced by scratching during the oxide forming process, a typical finite element model constructed for the wide plate tensile specimen (W=1 mm, H=2 mm) with a single edge shallow crack (crack length a=2 μm) was adopted in this study, as shown in Fig.2a and Fig.2c. x axis is the crack growth direction and θ is the angle around the crack front that rotates the ellipse center clockwise. It was assumed that the crack length a equals to 4, 3 and 2 μm, and the oxide thickness t at crack front was 1, 2 and 3 μm correspondingly in this study.

Generally, nickel-based alloy 600 is a power hardening material. The nonlinear relationship between stress and strain beyond yield is described by Ramberg-Osgood equation in this numerical simulation[12]:
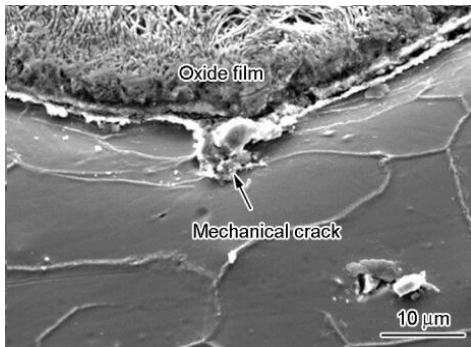
Fig.1　SCC induced by scratch[2]

$$\frac{\varepsilon}{\varepsilon_0} = \frac{\sigma}{\sigma_0} + \alpha \left(\frac{\sigma}{\sigma_0} \right)^n \qquad (10)$$

where ε is the total strain, including elastic and plastic strain; σ is the total stress; ε_0 is the material yield strain; σ_0 is the material yield stress; α is the offset coefficient and n

is the strain hardening exponent.

The alloy 600 at high temperature (288 ℃) in PWR primary water was used as the base metal in the simulation. The formed oxide was simplified as Cr_2O_3 considering that only a thin chromium oxide layer was formed at alloy 600 surface[13]. The oxide was assumed as a dense elastic oxide material[14,15].

The mechanical properties of alloy 600 and its oxide formed in PWR primary water at 288 ℃ water environment are given in Table 1.

Table 1　Mechanical properties of alloy 600 and its oxide formed in PWR primary water at 288 ℃ [16]

Material parameter	Alloy 600	Oxide
Young's modulus, E/GPa	190	19
Poisson's ratio, ν	0.286	0.3
Yield strength, σ_0/MPa	436	--
Yield offset, α	5.29	--
Hardening exponent, n	1	--

Fig.2　Finite element model: (a) whole specimen, (b) local crack front, and (c) morphology of the oxide

2.2　Finite element model

The typical finite element model in Fig.2a contains 7482 8-node biquadratic plane strain elements. Due to the large stress gradient near the interface between oxide and nickel-based alloy, a more refined mesh is adopted near the oxide around the crack front in the sub-model, in order to obtain more detailed and accurate data. The typical finite element model in Fig.2b contains 19856 8-node biquadratic plane strain elements. Through mesh sensitivity analysis, the minimum size of the element is 0.05 μm in the local crack front model.

The driving force of SCC crack initiation, which is independent of the external load, is mainly due to the film-induced stress generated during the oxide forming. The growth process of oxide was simulated by expansion. The thermal expansion coefficient β and the temperature

difference ΔT was assumed to be 0.001 and 6 ℃, respectively. Thus, the calculated film-induced stress on the oxide was obtained as σ_P =30 MPa[5, 6].

3　Results and Discussion

3.1　Effect of distance on stress-strain distribution of alloy 600

The variation of tensile stress with distance r ahead of crack front in the presence of a fixed film-induced stress is illustrated in Fig.3. For a specimen with a fixed oxide thickness t=3 μm as the same film-induced stress loaded, tensile stress decreases with the increasing distance. When the distance ahead of the crack front is relatively small (r<1 μm), the tensile stress right ahead of the middle part of the crack front and the compressive stress at the upper and

lower crack front both increases rapidly, and thus leads to the opening of middle part in the semi-elliptical crack front.

Fig.4 shows the tensile plastic strain distribution around the crack front within the range of $-90° \leq \theta \leq 90°$ at different distance r. The strain is greatly influenced by the distance ahead of the crack front. When the distance ahead of the crack front is very small ($r<0.5$ μm), the maximum tensile strain appears at the crack front midpoint, and the tensile plastic strain decreases rapidly with the increasing of distance r. As the distance r increases (0.1 μm$<r<$1 μm), the maximum strain moves to the upper and lower part of the crack front probably at $\theta=\pm15°$. The strain is very small and nearly close to zero around the crack front when $r>1$ μm.

Comparing Fig.4 with Fig.3, the stress and strain gradient are both obviously high when 0.1 μm$<r<$1 μm. The base metal is subjected to much higher tensile stress in the range of $-15° \leq \theta \leq 15°$. However, negative tensile strain appears in the range of $-90° \leq \theta \leq -15°$ and $15° \leq \theta \leq 90°$. It can be deduced that the compressive stress gives rise to compressive strain. The upper and lower part of crack front suffers compressive stress, which will result in a smaller amount of compressive strain to prompt the SCC crack propagating at the middle part of the crack front. The film-induced stress, or the wedge force, plays a major role in the SCC behavior of local zone very close to the crack front. However, the role of film-induced stress leading to crack growth becomes smaller with the increasing of distance r, and the crack growth will mainly depend on the higher applied loads.

3.2 Effect of oxide morphology on tensile stress of alloy 600

With different surface oxide morphology induced by scratch at the same film-induced stress, the tensile stress ahead of the crack front in the base metal can be seen from Fig.5. As the oxide thickness increases, the tensile stress ahead of the crack front also increases. Meanwhile, the larger the distance ahead of the crack front, the smaller the tensile stress is. It also shows that the tensile stress gradient decreases with the decreasing of oxide thickness, which
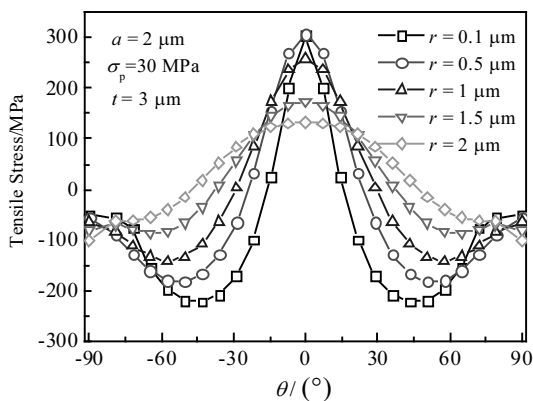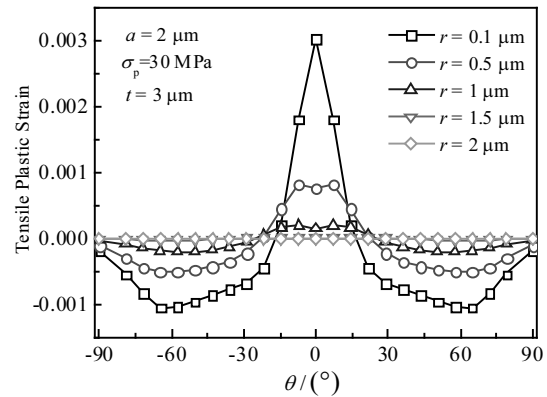
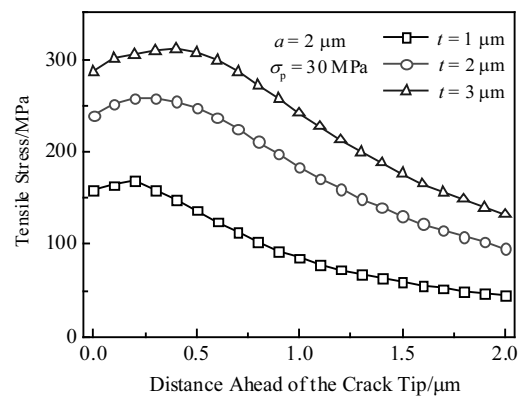Fig.4   Distribution of tensile plastic strain ahead of crack front

Fig.5   Tensile stress ahead of the crack front

indicates that the crack with thicker oxide is easy to crack and extend.

In Fig.4, the plastic strain distribution is greatly influenced by the distance r ahead of crack front. The plastic strain can differ hundreds of times with the increasing of distance r; thus it is important to determine the characteristic distance r_0 when using Eq.(9). The uncertain parameter r_0, which is the characteristic distance away from the growing crack front, could be determined by the curve fitting the experimental results to the numerically calculated CGR. The experimental results indicate that r_0 is on the order of several micrometers[11]. Considered the small geometric size of the wide plate tensile specimen, r_0 is assumed to be smaller than 1 μm.

In Fig.5, the maximum stress around the crack front ($t=1$ μm) appears at the distance $r=0.2$ μm, which can be considered to be the smallest size of passive zone. It is believed that the characteristic distance r_0 is less than the passive zone size. It should be noted that the values of stress and strain depend on the choice of the characteristic distance r_0. This does not affect the comparisons here when the specimens vary in oxide thickness. Therefore, a characteristic distance r_0 is set to be 0.2 μm in the following calculations.

Fig.3   Distribution of tensile stress ahead of crack front

Fig.6 shows the distribution of local tensile stress around the crack front in the range of −90°≤θ≤90°. In this figure, the maximal tensile stress around the crack front appears at θ=0°, where is the direction right in front of the crack front midpoint. The thicker oxide layer due to scratch can induce larger tensile stress. The stress difference around the crack front is the smallest when t=1 μm. The middle part of crack front is affected by the tension stress while the upper and lower crack front are affected by the compressive stress, which may make the middle part of the crack front rupture firstly and the tensile stress corrosion is easy to be generated. Large stress concentration at the crack middle part can also form microcracks. The wedge force eventually leads to the initiation and propagation of SCC crack. The magnitude of the local wedge force at crack tip is affected by the oxide thickness. Greater oxide thickness of scratch crack can induce greater wedge force. When the stress is great enough, the oxide film will rupture and crack. Finally, the SCC cracks initiate and propagate.

3.3 Effect of oxide morphology on tensile plastic strain of alloy 600

Fig.7 shows the tensile plastic strain along the ligament with different surface oxide morphology. The oxide can be considered to be a deformed hardening layer near scratch. The tensile plastic strains decrease rapidly with the increasing distance ahead of the crack front in a narrow area. But their values quickly converge to zero for the case of r≥1.5 μm. The tensile plastic strain increase with the increasing of oxide thickness. When the plastic strain accumulates to a certain extent, the oxide film will rupture and crack lead to cracking.

Fig.8 shows the distribution of tensile plastic strain around the crack front in the range of −90°≤θ≤90°. The maximum value of tensile strain appears at the crack front midpoint, which indicates that the midpoint of the crack front will be apart firstly. The base metal is subjected to tensile plastic strain when −15°≤θ≤15°. As the oxide film grows, the crack-front plastic strain gradually changes from tensile plastic strain to compressive plastic strain in the range of −90°≤θ≤−15° and 15≤θ≤90°. The tensile and
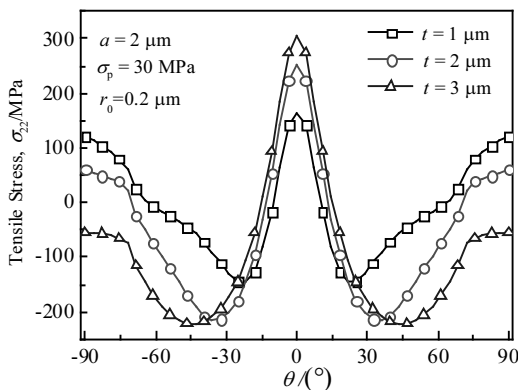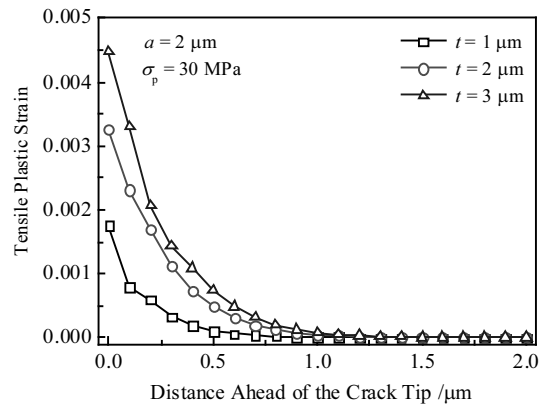
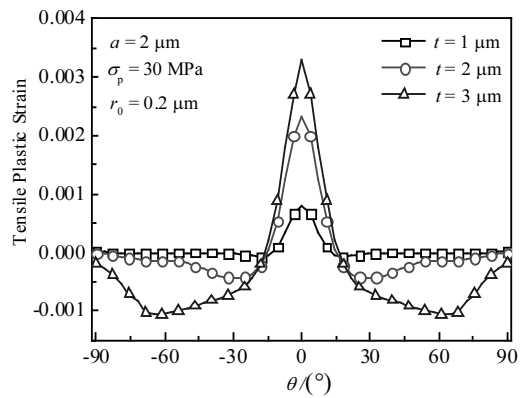Fig.7　Tensile plastic strain ahead of the crack front

Fig.8　Tensile plastic strain around the crack front

compressive plastic strain both increase with the increasing of oxide thickness. Comparing Fig.8 with Fig.6, the upper and lower part of the crack front suffers compressive stress, and it can be deduced that the higher compressive stress will cause the compressive strain, thus promoting the crack initiation and growing.

3.4 Effect of oxide morphology on tensile plastic strain gradient of alloy 600

Fig.9 shows the effect of oxide thickness on tensile plastic strain gradient ahead of the crack front along the ligament. Comparing Fig.9 with Fig.7, it is indicated the plastic strain and plastic strain gradient can differ hundreds to thousands of times with the increasing of distance r. The tensile plastic strain gradients decrease greatly with the increasing distance ahead of the crack front in a narrow area, but the strains quickly converge to the appropriate values when r≥1.5 μm. In general, the tensile plastic strain gradient of thicker oxide film is higher than that of the thinner.

Fig.10 shows the distribution of tensile plastic strain gradient around the crack front in the range of −90°≤θ≤90°. The maximum strain gradient appears at the upper and lower part of the crack front (θ=±15°) instead of at the crack front midpoint, and the strain gradient increases rapidly with the increasing of oxide thickness. Comparing Fig.5, Fig.6 and

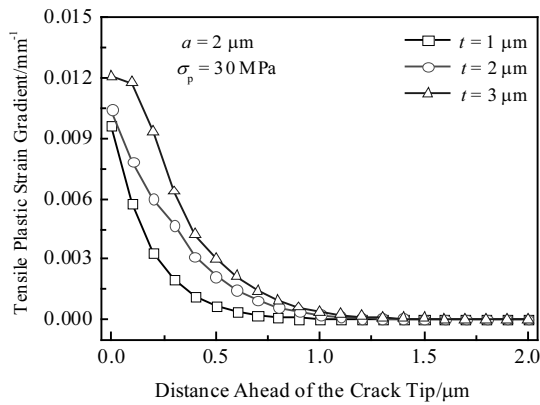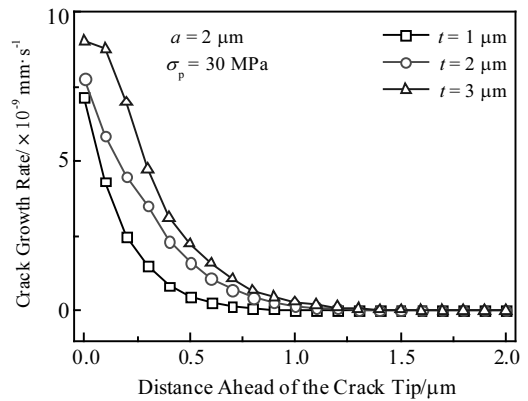Fig.6　Tensile stress around the crack front

Fig.9　Tensile plastic strain gradient ahead of the crack front

Fig.11　Crack growth rate ahead of the crack front

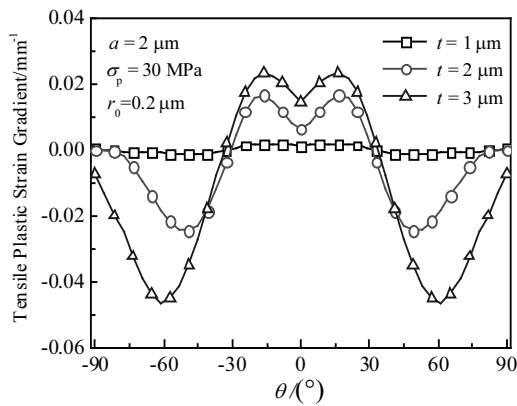Fig.10　Tensile plastic strain gradient around the crack front

the CGR increases rapidly with the increasing of oxide thickness. In Fig.12, the CGR at the crack front midpoint is slightly lower, but the stress and strain at the crack front midpoint is the maximum in Fig.6 and Fig.8. It can be deduced that although the crack front midpoint may separate firstly, its growth rate is slower than that of the crack front middle part ($\theta=\pm15°$). The propagation of the crack front ($-30°\leq\theta\leq30°$) will promote the cracking of the crack middle part. In addition, since the tensile strain gradient is less than zero in the range of $-90°\leq\theta\leq-30°$ and $30°\leq\theta\leq90°$, there is almost no crack growth in the upper and lower part of crack front. The reason why the stress and strain are in the range of $-90°\leq\theta\leq-30°$ and $30\leq\theta\leq90°$ are not the tensile stress and strain, which are the crack driving force, but the compressive stress and strain.

Fig.10, it can be deduced that compressive stress will cause compressive strain and negative strain gradient, which will be an obstacle of SCC crack propagating in the upper and lower part of the crack front ($-90°\leq\theta\leq-30°$ and $30°\leq\theta\leq90°$).

3.5　Effect of oxide morphology on CGR of alloy 600

For a regular electrochemical environment where the crack tip is exposed, the plastic strain gradient is essentially consistent with CGR. The strain gradient at crack tip is usually used as a unique factor to describe the mechanical condition in Eq.(9). The oxidation rate constant κ_a' is taken to be 7.478×10^{-7}[17], and the exponent of the current decay curve m is given as 0.5 in Eq.(9)[11]. Substituting the value of $d\varepsilon_{22}/dr$ (at a characteristic distance $r_0 =0.2$ μm) into Eq.(9), the CGR ahead of the crack front can be obtained in Fig.11. Its CGR decreases greatly with the increasing distance ahead of the crack front in a narrow area. But their values quickly converge to zero when $r\geq1.2$ μm. The CGR increases with the increasing of oxide thickness.

To analyze the effect of oxide thickness on SCC crack growth rate, the CGR around the crack front in the range of $-90°\leq\theta\leq90°$ is shown in Fig.12. When the tensile plastic strain gradient is negative, the corresponding CGR equals to zero in Fig.10. Close to the middle part of crack front, the crack growth rates reach their maximum when $\theta=\pm15°$. And
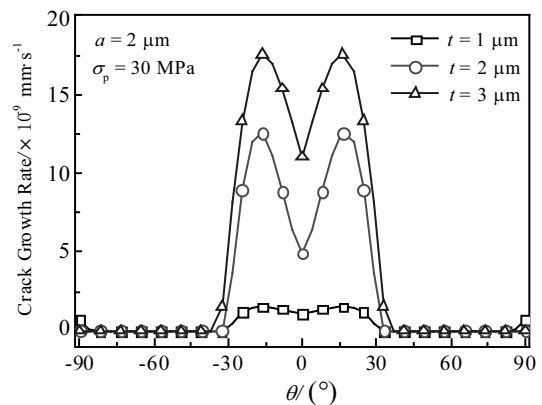

Fig.12　Crack growth rate around the crack front

4　Conclusions

1) The film-induced stress, or the wedge force, is a very major crack driving force in SCC. However, the role of film-induced stress in crack growing becomes smaller and smaller with the increasing distance, but increasingly dependent on high applied loads.

2) A large stress concentration at the crack front midpoint can form micro cracks in the oxide. The local wedge force affected by the oxide thickness leads to the initiation and propagation of SCC. Greater oxide thickness of scratched crack can give rise to wedge force.

3) The tensile and compressive plastic strain both increase with the increasing of oxide thickness. The negative tensile strain gradient appears in the range of $-90°\leq\theta\leq-30°$ and $30°\leq\theta\leq90°$. Compressive stress causes compressive strain and negative strain gradient, which will be an obstacle of SCC crack propagating in the upper and lower part of the semi-elliptical crack front.

4) In a small range around crack front, the tensile strain and tensile plastic strain gradient around the crack front increase with the increasing of oxide thickness. Though the crack front midpoint may separate firstly, its growth rate is slower than that of the crack front middle part($\theta=\pm15°$). The propagation of the upper and lower crack front will prompt the cracking of the crack middle part. There is almost no crack growth in the range of $-90°\leq\theta\leq-30°$and $30°\leq\theta\leq90°$.

References

1　Meng F J, Wang J Q, Han E H *et al*. *Acta Metallurgica Sinica* [J], 2011, 47(7): 839 (in Chinese)

2　Meng F J, Wang J Q, Han E H *et al*. *Journal of Chinese Society for Corrosion and Protection*[J], 2013, 33(5): 413 (in Chinese)

3　Ding X S. *Corrosion & Protection*[J], 2007, 28(7): 364 (in Chinese)

4　Ding X S. *Corrosion & Protection*[J], 2002, 23(10): 441 (in Chinese)

5　Li J X, Wang Y B, Qiao L J *et al*. *Acta Metallurgica Sinica*[J], 2002, 38(8): 861 (in Chinese)

6　Li J X, Gao K W, Su Y J *et al*. *Scientia Sinica (Technologica) (Series E)*[J], 2003, 33(9): 796 (in Chinese)

7　Xue H., Ogawa K, Shoji T. *Nuclear Engineering and Design*[J], 2009, 239(4): 628

8　Ford F P. *Corrosion*[J], 1996, 52(5): 375

9　Shoji T, Lu Z P, Murakami H. *Corrosion Science*[J], 2010, 52(3): 769

10　Xue H, Shoji T. *Journal of Pressure Vessel Technology, Transations of the ASME*[J], 2007, 129(3): 460

11　Peng Q J, Kwon J, Shoji T. *Journal of Nuclear Materials*[J], 2004, 324(1): 52

12　Ramberg W, Osgood W R. *Tech Note, No. 902*[R], Washington, DC: NACA, 1943

13　Panter J, Viguier B, Cloué J M *et al*. *Journal of Nuclear Materials*[J], 2006, 348(1-2): 213

14　Tan Y, Liang K X, Zhang S H. *Journal of Chinese Society for Corrosion and Protection*[J], 2013, 33(6): 491 (in Chinese)

15　Lu Y H, Peng Q J, Sato T *et al*. *Journal of Nuclear Materials*[J], 2005, 347(1-2): 52

16　Xue H, Li Y Q. *Rare Metal Materials and Engineering*[J], 2016, 45(3): 537

17　Xue H, Sato Y, Shoji T. *Journal of Pressure Vessel Technology*[J], 2009, 131(1): 011 404

划痕诱发的镍基合金应力腐蚀裂尖扩展驱动力分析

赵凌燕，崔英浩，杨富强，薛　河

(西安科技大学，陕西 西安 710054)

摘　要： 为了解表面划伤导致的不同氧化物形貌对镍基合金应力腐蚀 (SCC) 行为的影响，模拟了膜致应力下镍基合金划伤裂纹尖端的局部应力应变场。结果表明，楔形力是引发 SCC 裂纹扩展的主要驱动力。划痕裂纹前端的氧化物越厚，楔形力越大，并会增大 SCC 裂纹扩展速率。裂尖氧化物的形成导致了压应力、压应变和负的应变速率，并会阻碍半椭圆裂纹尖端上部和下部的 SCC 裂纹扩展。

关键词： 镍基合金；划痕；氧化物形貌；楔形力；裂纹扩展速率

作者简介：赵凌燕，女，1978 年生，博士，副教授，西安科技大学理学院，陕西 西安 7100154，电话：029-85583132，E-mail: gloomy2@foxmail.com